Design and optimization of nature-inspired polygon-based lattice structures for lightweight and high-strength applications

CHOUHAN, Ganesh <http://orcid.org/0000-0002-1098-5793>, CHALISGAONKAR, Rupesh, PUROHIT, Anshuman, NAMDEO, Avinash Kumar <http://orcid.org/0000-0001-9486-0412>, YADUWANSHI, Deepak Kumar, GANDVANE, Kunal <http://orcid.org/0009-0008-0023-7063> and BIDARE, Prveen <http://orcid.org/0000-0003-2852-3498>

PAPER • **OPEN ACCESS**

Design and optimization of nature-inspired polygon-based lattice structures for lightweight and high-strength applications

Materials Research Express

OPEN ACCESS

RECEIVED
29 September 2025

REVISED
8 November 2025

ACCEPTED FOR PUBLICATION
5 December 2025

PUBLISHED
7 January 2026

PAPER

Design and optimization of nature-inspired polygon-based lattice structures for lightweight and high-strength applications

Ganesh Chouhan[1,*], **Rupesh Chalisgaonkar**[1], **Anshuman Purohit**[1], **Avinash Kumar Namdeo**[2], **Deepak Kumar Yaduwanshi**[1,2], **Kunal Gandvane**[3] and **Prveen Bidare**[4,*]

[1] Department of Mechanical Engineering, Medi-Caps University, Indore, India
[2] Department of Mechanical Engineering, Lingaya's Vidyapeeth, Faridabad, India
[3] Department of Civil Engineering, Indian Institute of Technology Bombay, Mumbai, 400076, India
[4] School of Engineering and Built Environment, Sheffield Hallam University, Sheffield S1 1WB, United Kingdom
[*] Authors to whom any correspondence should be addressed.

E-mail: p.bidare@shu.ac.in

Keywords: bio-inspired design, polygon-based lattice structures, additive manufacturing, stereolithography (SLA), strength-to-weight ratio

Abstract

Additive manufacturing stands at the cutting edge of modern production, enabling the fabrication of intricate geometries such as lattice structures with superior stiffness-to-weight ratios that are often unattainable through conventional methods. This study focuses on the development and evaluation of polygon-based lattice structures inspired by naturally occurring botanical forms, known for their efficient load distribution and structural connectivity. Square, triangular, and pentagonal unit cells were systematically designed across three porosity levels (50%, 55%, and 60%) to investigate the influence of geometry on mechanical performance. High-resolution stereolithography (SLA) 3D printing was employed to fabricate the samples, ensuring precision in capturing fine lattice details critical for accurate mechanical assessment. Finite Element Analysis (FEA) was employed to evaluate the mechanical performance of bio-inspired lattice structures under multidirectional compressive loading. The investigation integrated both computational simulations and experimental testing to validate structural behavior. Among the configurations studied, the pentagon geometry with 50% porosity lattice exhibited the best compressive performance, with a peak strength of 40.1 MPa, which is 62% higher than the 50% square lattice and 170% higher than the 60% triangle lattice. Additionally, Scanning Electron Microscopy (SEM) analysis was conducted to examine fracture mechanisms and microstructural integrity.

1. Introduction

One of the most pressing issues in the mechanical engineering today is that of optimizing the strength-to-weight ratio of components to an optimal level for modern engineering application such as structural performance. This issue results from the simultaneous requirement for lighter mechanical systems to increase efficiency and performance, yet also be able to support imposed loads and function safely under harsh conditions and provide combine structural efficiency, energy absorption, and sustainability [1]. Conventional manufacturing technologies have traditionally difficulty addressing these mutual demands, for which sophisticated manufacturing techniques, revolutionary lattice configurations, and comprehensive test methods need to be utilized for producing lightened components while sustaining the strength and structural integrity [2, 3]. Lattice structures inspired by natural designs offer a promising solution to achieve the required performance in modern engineering applications. The advanced additive manufacturing (AM) technology has thus emerged as an unprecedented tool through which challenging porous bio-inspired geometric features could now be made readily achievable by virtually unmanufacturable methods [4, 5].

Bio-inspired structures in additive manufacturing are excises in multiple scales (nano, micro, meso, macro) and include composite materials (mineralized and non-mineralized), porous designs for lightweight [6], resilience and tough applications, interfaces for crack deterrence, and shape-changing structures for adaptive functionality [7–9].

These structures draw from natural systems like bamboo, horsetail plants, beetle forewings, tendons, luffa, pomelo, mantis shrimp, woodpecker's beak, and leaves, gives innovative solutions for improved mechanical properties, energy absorption, fluid flow optimization, and multifunctional applications in novel and challenging fields. Therefore, lattice structures are geometric frameworks inspired by natural designs, such as trabecular bone, honeycombs, or spider webs, which provide promising solution to achieve customizable and superior properties for high strength-to-weight ratio, energy absorption, and multifunctional applications [10, 11].

In additive manufacturing, a lattice is a three-dimensional framework composed of interconnected unit cells with diverse geometric configurations, such as polygons to produce through computer-aided design (CAD) software and frequently combined to create a 3D-printed part. These parts are engineered to mimic natural load-bearing architectures, enabling lightweight, high-strength, and multifunctional applications across various industries. Polygon-based lattice structures, including honeycomb, triangular, square, Kagome, gyroid, and octet truss with different cell size/shape, strut thickness and porosity configuration to optimize mechanical, thermal, and fluid flow properties. For example, sea urchin-mimetic open-cell porous microstructures illustrated that bending stiffness, maximum load, and energy absorption are notably affected by geometrical parameters and porosity [12]. Likewise, butterfly wing-mimetic gyroid structures reinforced with carbon fiber-reinforced polymer (CFRP) rods showed more than double the stiffness (46 N mm^{-1}) than unreinforced structures (20 N mm^{-1}) [13]. These results demonstrate the potential of bio-inspired gyroid structures to improve mechanical performance, making them ideal for applications that need lightweight, high-strength, and energy-efficient materials. Likewise, multi-cell bamboo fiber-inspired designs exhibited a specific energy absorption (SEA) four times higher than conventional structures under both lateral and axial impact loads [14], while structures mimicking the vascular tube distribution of bamboo showed a 1.24 times higher load-bearing capacity compared to regular tube designs [15]. Beetle forewing-inspired honeycomb patterns achieved an SEA of 35 J g^{-1}, surpassing traditional metallic honeycomb structures [16]. Additionally, hierarchical multi-cell porous structures inspired by tendons and other natural geometries revealed that parameters like cell number, wall thickness, and diameter significantly influenced crashworthiness, with SEA values reaching up to 1.6 kJ kg^{-1} for foam-filled designs [17–19]. Further studies highlighted SEA improvements of 9.79% to 68.33% in bio-inspired designs compared to conventional structures [20, 21], with quadrilateral, hexagonal, and octagonal cross-sections achieving SEA values of 29.94 kJ kg^{-1}, 33.86 kJ kg^{-1}, and 36.09 kJ kg^{-1}, respectively, significantly higher than non-tubular designs (22.99 kJ kg^{-1}) [22]. These findings underscore the potential of bio-inspired tubule structures to enhance energy absorption and stress distribution, making them ideal for applications requiring lightweight, high-performance materials.

Bio-inspired foam structures, drawing inspiration from natural sources such as luffa, pomelo, lotus root, turtle shells, and bone, have shown remarkable improvements in mechanical properties, particularly in energy absorption and stress distribution. For instance, luffa-inspired spongy structures with macro- and micro-pores demonstrated a peak force of 333.9 kN, significantly higher than conventional foam cylinders (199.7 kN) [23]. Pomelo peel-inspired foam structures, incorporating fiber bundles, exhibited a 30% increase in stiffness and higher plateau stress compared to standard foam designs [24]. Lotus root-inspired microstructures, characterized by long cylindrical pores, displayed unique deformation behaviors, with slip deformation observed when tested parallel to the pore direction [25]. Turtle shell-inspired closed-cell foam networks achieved higher specific energy absorption (SEA) than other natural large-cell foam designs [26], while bone-inspired graded pore structures in foam-filled tubes showed up to 24% greater SEA compared to uniform foam-filled tubes [27]. These findings highlight the potential of bio-inspired foam structures to enhance energy absorption, stiffness, and stress management, making them suitable for applications requiring lightweight and high-performance materials.

Bio-inspired sandwich panel structures, inspired by natural systems such as the mantis shrimp, woodpecker's beak, and leaves, have demonstrated significant enhancements in crashworthiness, energy absorption, and structural stiffness. For example, mantis shrimp-inspired corrugated structures with the integration between impact layers to significantly enhance crash load resistance while notably reducing the initial peak impact force [28]. Similarly, the specific energy absorption of porous honeycomb structures model has inspired from woodpecker beaks which shows 1.25 times more than that of conventional honeycomb [29] sandwich panels with the same core thickness [19]. Moreover, leaf-inspired structural designs have mimic the orientation of porous vascular bundles to provide a 5.3% increase in stiffness, along with enhanced energy absorption and critical buckling load compared to traditional honeycomb core structures without grid reinforcement [30]. These results show the significant potential and scope of bio-inspired sandwich panels to enhance mechanical performance under different load condition, design them for highly suitable for applications that need lightweight, high-strength, and sufficient energy-absorbing materials and structure.

In additive manufacturing, a lattice is a complex, three-dimensional structure which is designed and drafted by using computer-aided design (CAD) software and frequently used in combination with 3D-printed object or component. These components are made-up of a network of interconnected structures arranged in a repeating pattern throughout the object for maintaining the mechanical stability and robustness. By changing

and modifying the porosity levels, material consumption may be efficiently decreased, total weight can be decreased, and mechanical qualities like stiffness and impact resistance can be enhanced. Natural materials like sea urchin spines and butterfly wings are used to create bio-inspired gyroid structures, which have demonstrated impressive gains in mechanical characteristics, especially in bending stiffness, load-bearing capacity, and energy absorption. For example, open-cell porous microstructures modelled after sea urchins showed that porosity and geometrical parameters have a major impact on energy absorption, maximum load, and bending stiffness [31]. Similarly, carbon fiber-reinforced polymer (CFRP) rod-reinforced gyroid structures that resembled butterfly wings demonstrated more than double the stiffness (46 N mm^{-1}) in comparison to non-reinforced structures (20 N mm^{-1}) [32]. These results demonstrate how bio-inspired gyroid structures can improve mechanical performance, which makes them appropriate for uses requiring materials that are strong, lightweight, and energy-efficient.

Bio-inspired porous structures have shown remarkable mechanical capabilities, making them perfect for high-performance applications. These structures imitate natural designs found in sea urchins, horse hooves, trabecular bone, butterfly wings, and beetle exoskeletons. The promise for lightweight, high-strength designs was demonstrated by sea urchin-inspired gyroid structures, which demonstrated enhanced bending stiffness and energy absorption with higher porosity [31]. Due to sequential buckling and collapse mechanisms, horse hoof-inspired tube constructions showed a 69% improvement in energy absorption and a 29% decrease in peak force, demonstrating their better crashworthiness [33]. Trabecular bone-inspired foam structures absorbed the highest energy at a 70° layer angle, with increasing layer thickness enhancing peak force and energy absorption, making them suitable for impact-resistant applications [34]. Butterfly wing-inspired gyroid structures reinforced with carbon fiber-reinforced polymer (CFRP) rods showed twice the stiffness (46 N mm^{-1}) compared to non-reinforced designs (20 N mm^{-1}), emphasizing the benefits of bio-inspired reinforcement [32]. Additionally, beetle-inspired honeycomb structures displayed a stress–strain plateau region under compression, optimizing material strength and stability, which is critical for aerospace and automotive applications.

These structures were fabricated using various additive manufacturing (AM) techniques, each with its own benefits and drawbacks. Material extrusion, using materials like ABS, PLA, and tough nylon, offers low cost and simplicity but suffers from weak mechanical properties and coarse resolution [31–34] . Material jetting, employing materials such as Vero White Plus and Tango Plus, provides fine resolution and high-quality prints but is expensive and limited in material options [35, 36]. Vat polymerization, using photopolymerizable acrylic resin, enables the production of complex geometries with high precision but is slow and costly [32]. Powder bed fusion, utilizing titanium alloy (Ti-6Al-4V) and amorphous calcium polyphosphate (CPP), delivers high-quality, high-strength parts but is expensive and prone to high porosity in binder-based methods [37, 38].

The integration of bio-inspired designs with AM technologies has opened new possibilities for applications in energy absorption, load-bearing, and tissue engineering. For example, trabecular bone-inspired foam structures demonstrated efficient compressive strength due to anisotropic fracture toughness, making them suitable for bone defect repair and regeneration [39]. Similarly, bone-inspired designs promoted stable crack propagation and reduced stress concentrations, enhancing structural integrity under dynamic loading [38]. These findings underscore the potential of bio-inspired porous structures to revolutionize lightweight, high-performance material design, with future research focusing on optimizing material formulations and AM processes for broader industrial applications.

This study investigates three polygon-based lattice structures, namely triangle, square, and pentagon, that have not been comparatively explored in the context of compressive loading. Samples were fabricated using vat photopolymerization additive manufacturing, selected for its superior geometric accuracy over other commonly used AM techniques. The mechanical performance of the lattices was evaluated through compressive strength, energy absorption, and strength-to-weight ratio measurements, along with detailed stress–strain analysis. Additionally, microstructural examination was conducted to assess fracture behavior and surface characteristics, providing insights into material integrity and failure mechanisms.

2. Material and methods

This section outlines the conceptual framework of the study, detailing the design methodologies for the three lattice geometries triangular, square, and pentagonal and their fabrication using Stereolithography (SLA) additive manufacturing. The process includes both preprocessing (model preparation and slicing) and postprocessing (cleaning and UV curing) steps to ensure geometric fidelity and structural consistency. Furthermore, the boundary condition setup for Finite Element Analysis (FEA) is presented to simulate the compressive response of the structures. Scanning Electron Microscopy (SEM) analysis methodology is also described for evaluating the microstructural characteristics and fracture behavior of the printed lattices.

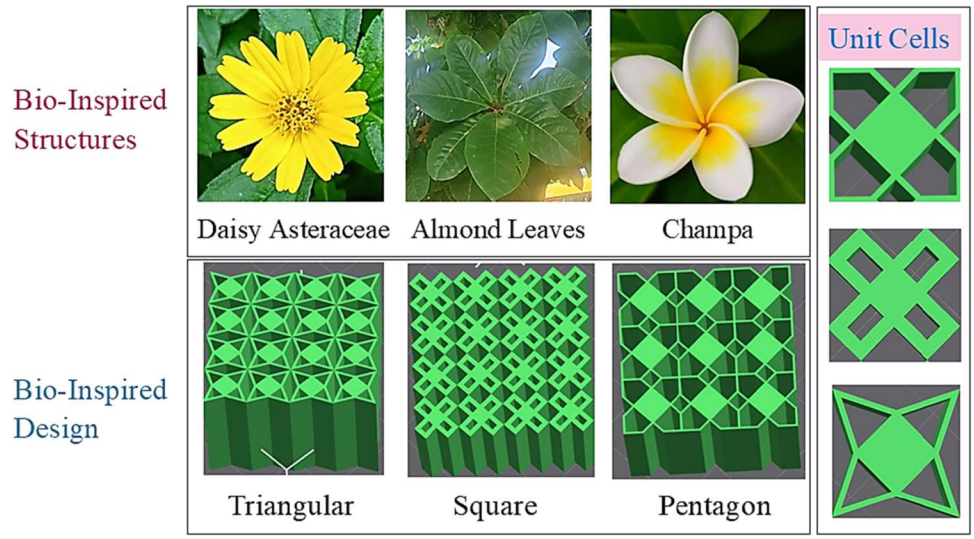

Figure 1. Botanical elements with connecting structures.

2.1. Ideation and design

Our project began with a close observation of natural environments, focusing on the complex geometrical patterns of nature's optimized biological structures and integrating them into bio-inspired lattice designs. Nature provides a treasure trove of optimized designs, especially in plant elements like flowers, leaves, and branches, where the connecting structures and unit cell multiplications are the basis of mechanical strength, stability and flexibility. By closely observing botanical structures such as the radial symmetry of Sphagneticola trilobata (Creeping Daisy), the spiral phyllotaxy of Terminalia catappa (Indian Almond Tree), and the organic curvature of Plumeria alba (White Frangipani), we designed three distinct lattice frameworks: rectangular, triangular, and pentagon-extended-to-rectangle as shown in figure 1. These observations motivated us to develop bio-inspired lattice structures, utilized the natural efficiency of biological geometries in engineering.

Understanding that the multiplication of polygon shapes unit cells and structural connectivity are essential to ensure stability and mechanical performance by leveraging the emulate nature's intrinsic design principles. Polygons, such as rectangles, triangles, and pentagons, provide a balance between simplicity and complexity, enabling the creation of lightweight yet robust frameworks. The rectangular lattice, which takes cue from the radial symmetry and petal structure of Sphagneticola trilobata (Creeping Daisy), is characterized by even load distribution, high stiffness, and impact resistance, and thus is suitable for energy-absorbing structures and biomedical devices. The triangular lattice, which is based on the spiral phyllotaxy of Terminalia catappa (Indian Almond Tree) leaves, exhibits increased structural strength, high compressive strength, and maximized stress distribution, making it a prime candidate for lightweight aerospace and automotive parts. Finally, the pentagon-extended-to-rectangle lattice, which mimics the organic curve and symmetric petal shape of Plumeria alba (White Frangipani), provides an optimal tradeoff of flexibility, failure resistance, and mechanical resilience and hence can be applied to biomedical scaffolds and adaptive load-bearing applications. Such bioinspired structures point towards the strength of nature-inspired innovation for the production of high-performance, application-driven materials. These structures were then developed further with stereolithography (SLA) 3D printing and tested under axial compression testing and numerical simulations, validating their viability for biomedical, aerospace, and lightweight structural component applications.

The lattice structures under consideration are designed using polygonal hollow units such as triangles, squares, and pentagons, that form the fundamental building blocks of the geometry. These units are interconnected through a network of beams or struts, creating a grid-like or spatially periodic framework that effectively balances stiffness and lightweight characteristics. Figure 2 illustrates representative polygonal hollow geometries commonly employed in advanced engineering applications due to their optimized load distribution, high strength-to-weight ratios, and design adaptability.

2.2. Analytical framework for hollow polygonal lattice designs

The analytical framework of targeted structures composed of polygonal hollow configurations entails the formulation of mathematical frameworks that accurately characterize their geometric and mechanical behavior. Such modeling is fundamental for predicting structural responses under various loading conditions

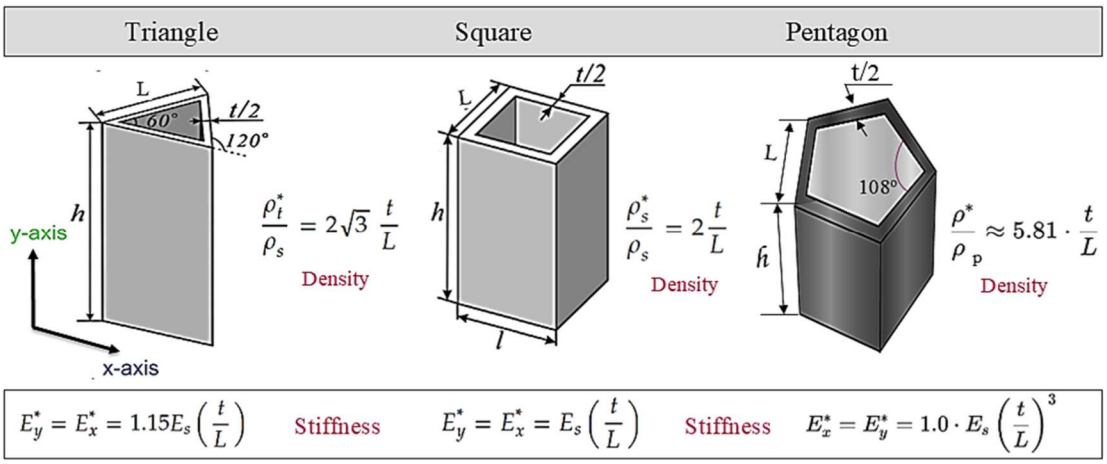

Figure 2. Unit cells of selected polygon lattices with density and stiffness equations.

and serves as a vital tool for engineers and designers in the optimization of advanced structural systems. Three distinct polygonal unit cell configurations triangle, pentagon, and square were geometrically defined to establish the fundamental parameters governing the structural characteristics of the lattice architectures and figure 2 presents the density equations. In these formulations, t denotes the thickness of the lattice wall, L signifies the edge length of the polygonal unit cell, and R corresponds to the radius of the encompassing circular boundary. The symbols ρ^* and ρs refer to the density of the polygon lattices and the solid cell walls. The specific porosity of various lattice geometries triangular (ρ^*t), square (ρ^*s), and pentagon (ρ^*p) are defined to facilitate comparative analysis across different structural configurations.

According to Gibson and Ashby [40], square hollow structures exhibit stiffness characteristics similar to triangular ones when both share the same relative density. These square configurations are particularly suited for applications where directional stiffness is desired, owing to their anisotropic nature. Structurally, the square unit cell features two pairs of parallel walls arranged at right angles. While one pair offers considerable resistance to in-plane loads, the opposing pair tends to flex more easily, making it vulnerable to transverse bending under planar loading conditions. The stiffness of lattice structures varies significantly with the geometry of the unit cell. Triangular hollow structures are typically stretch-dominated, offering the highest in-plane stiffness due to their fully triangulated geometry, which efficiently transfers loads through axial forces in the struts. In contrast, square hollow structures are bending-dominated and exhibit lower stiffness, as two of their walls are prone to transverse bending under in-plane loads. Pentagonal hollow structures, which often lack full triangulation and exhibit irregular load paths, also fall into the bending-dominated category. The pentagon used in the actual unit cell design is a modified form; however, the relative density and stiffness equations from the standard pentagon were used as an approximation.

To quantitatively evaluates the mechanical performance of the lattice structures, this study utilizes several key metrics, including Specific Energy Absorption (SEA), compressive strength, weight-to-strength ratio, and modulus. The Specific Energy Absorption (SEA) is defined as the energy absorbed per unit mass of the structure and EA is the total energy absorbed is calculated using the following expression:

$$EA = \int_0^X F(x)\,dx \tag{1}$$

$$SEA = \frac{EA}{M} \tag{2}$$

2.3. Simulation framework

Polygon based lattice were designed and analyzed for quasi-static axial compressive behavior and structural response within linear elastic limit using finite element modeling in nTopology Inc. (2023, New York, NY, USA). The simulation replicates the physical test circumstances by applying the proper boundary restrictions: The square lattice bottom surface is fixed and completely limited, while the upper part strikes the lattice at a steady 2 mm min^{-1} as shown in figure 3. To simulate realistic loading conditions, boundary constraints were applied by restricting lateral and longitudinal movements, with the bottom face fixed to represent a rigid support. For both experimental and numerical study, the 50KN load has been selected. To create a FE model, every polygon-based lattice has undergone meshing and refined meshing processes. Tetrahedron elements were selected in this study because of their ability to accurately capture complex lattice geometries where hexahedral meshing becomes challenging or impractical. Moreover, tetrahedral meshes provide greater flexibility for automatically generating

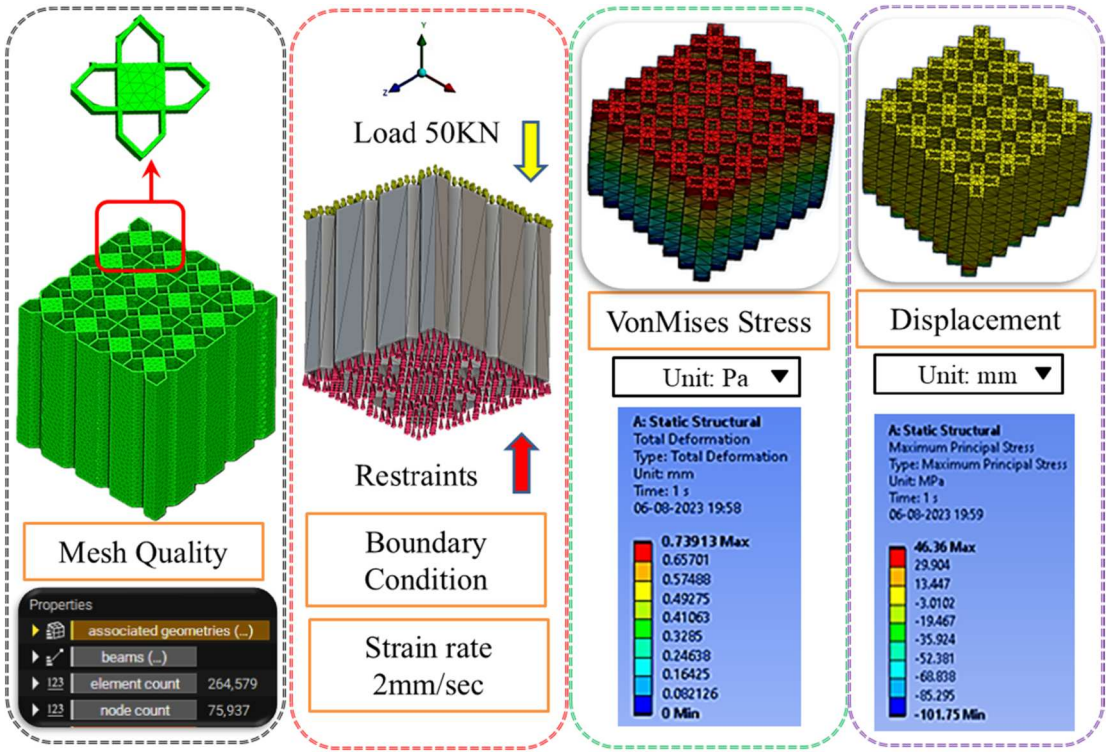

Figure 3. Boundary conditions applied to a lattice structure and the resultant reaction forces on the top surface of the lattice.

conforming meshes in intricate structures such as polygon-based lattices. An additional finite element (FE) volume mesh refinement was performed to achieve an optimal resolution of the von Mises stress distribution. A refined mesh with element sizes ranging from 0.25 to 0.5 mm was employed to capture the von Mises stress accurately. The final mesh for square ($4 \times 4 \times 4$) lattice consisted of 278,756 mixed-type elements and 78,298 nodes, providing sufficient resolution for stress analysis. The mesh generation and simulation required 00:10:14 and 00:14:11 (hh:mm:ss), respectively, reflecting the computational effort associated with the FEA process. The epoxy resin used exhibits a density of 1.05–1.25 g cm^{-3}, tensile strength of 32.52 MPa, and a modulus of elasticity ranging from 1.00 to 2.65 GPa. It has a Poisson's ratio of 0.389 and a melting point between 150 °C and 162 °C, making it suitable for structural and thermal applications in additive manufacturing.

2.4. Additive manufacturing of samples

In this work, three different BILS based unit cell were selected and designed as shown in table 1, to test axial compression and assess their mechanical performance, including load-bearing capacity, deformation behavior, and failure modes. Stereolithography (SLA) 3D printing, a high-precision additive manufacturing method, was used to create the intended lattice structures. With a printing size of $119 \times 65 \times 160$ mm, a print speed of 6–18 s/layer height, and a nominal power of 72 W, the Creality LD002R LCD 3D printer was utilized. The parent material, ELEGOO ABS Standard Photopolymer Resin (405 nm), offering very low volume shrinkage, high precision, excellent tensile strength, and a good modulus of elasticity. The resin exhibits a density in the range of 1.05–1.25 g cm^{-3}, a tensile strength between 32–52 MPa, and an elastic modulus ranging from 1.0 to 2.65 GPa. The material also shows a shrinkage of about 3.72%–4.24%, with elongation at break varying widely from 3.0% up to 150%, depending on curing conditions and testing methods. In addition, the melting temperature was considered in the range of 150 °C–162 °C. Figure 4 shows the printing method with and without the support system. Both printing positions had minor quality issues during the printing process. Total nine samples have been printed. After SLA printing, the samples were washed with isopropyl alcohol (IPA) to remove uncured resin, followed by post-curing under a UV laser. The support structures were then carefully removed using appropriate tools while ensuring safety. Although minor surface marks from the support contact points were observed, they did not significantly affect the overall geometry or integrity of the samples. The designs used in this study are complex, with thin sections at the corners. Printing without supports led to warping at the outer regions, and during removal from the build platform, some thin sections were damaged due to their fragile nature. The BILS samples were fabricated using 640 layers with a layer thickness of 0.050 mm, requiring a total build time of 2 h 9 m 52 s. The selection of layer thickness and the corresponding number of layers directly influences the surface finish, dimensional accuracy, and mechanical performance of the printed part.

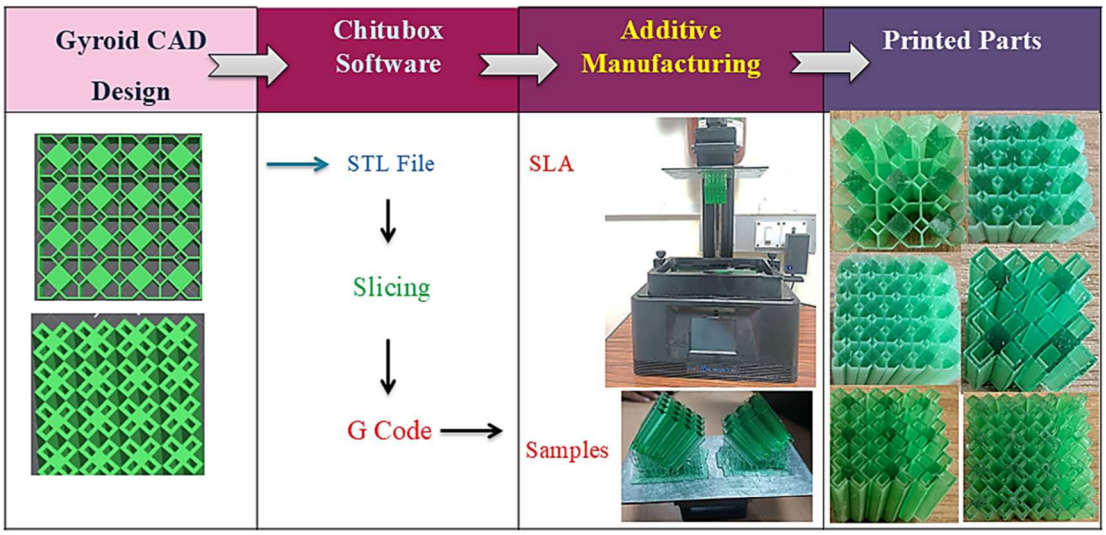

Figure 4. Steps to develop samples from design to physical form.

Table 1. Dimensions and design parameters of the bio-inspired lattice structures (BILS).

Geometry	Unit cell size (mm)	Wall thickness (mm)	Porosity (%)	Sample dimensions (mm)	Surface area (mm^2)
Square Lattice	4 × 4 × 4	0.8	50	30 × 30 × 30	33,000
	3 × 3 × 3		55		30,500
	2 × 2 × 2		60		29,000
Triangular Lattice	4 × 4 × 4	0.8	50		37,000
	3 × 3 × 3		55		35,000
	2 × 2 × 2		60		27,000
Pentagon Lattice	4 × 4 × 4	0.8	50		36,000
	3 × 3 × 3		55		33,000
	2 × 2 × 2		60		28,000

2.5. SEM analysis

To investigate the surface morphology of polygon-based lattice structures, high-resolution Field Emission Scanning Electron Microscopy (FESEM) was conducted. ABS-like resin samples were meticulously prepared following established metallographic protocols. Each specimen was sectioned into 1 × 1 cm^2 segments, cryogenically fractured to preserve the native fracture features, and sputter-coated with a thin layer of vanadium to ensure optimal imaging quality. The microstructural analysis was performed using an FEI Quanta 250 FEG FESEM system. This SEM image shows the fracture surface of a sample imaged at 5000× magnification using secondary electron mode (SE), under a 20.00 kV accelerating voltage and high vacuum conditions. The field of view reveals important microstructural features that provide insights into the fracture mechanism.

3. Result and discussion

3.1. Testing system and deformation behavior

The deformation behavior under quasi-static compressive load condition of SLA fabricated polygon-based lattice structures was investigated in uniaxial compression testing on a servo-hydraulic Instron 8801 universal testing machine with a maximum load capacity of 100 kN, as shown in figure 5. The test samples were placed between a fixed lower vice and a movable upper vice, while maintaining the same orientation of all the sample as maintain during the printing process. The compression tests were conducted in according the ASTM D695 standards [41] at a constant displacement rate of 2 mm min^{-1}. The termination condition was set, when either 80% deformation of the sample was reached or the reaction force exceeded 50 kN during the testing process. Under regulated testing circumstances, this setup made precise measurement of mechanical response under controlled conditions. After the test, the failed lattice fragments were collected and examine the deformed samples, as illustrated in figure 5(b). The deformation and failure patterns were analyzed to identify dominant failure modes such as layer-wise collapse, shear band formation, buckling, or crack propagation. These figments analysis are important for understanding the load-bearing capacity and mechanisms of polygon-

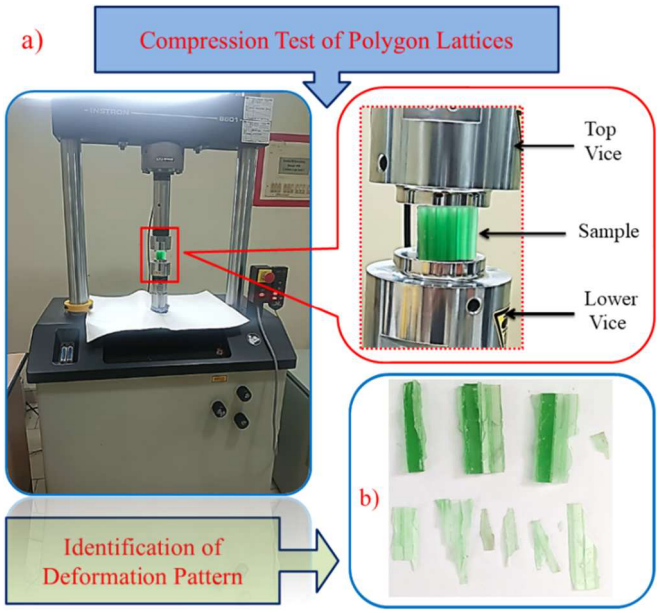

Figure 5. The schematic illustration of the compressive test under quasi-static load condition: (a) Compression tests of setup, (b) Deformation pattern in lattice structure.

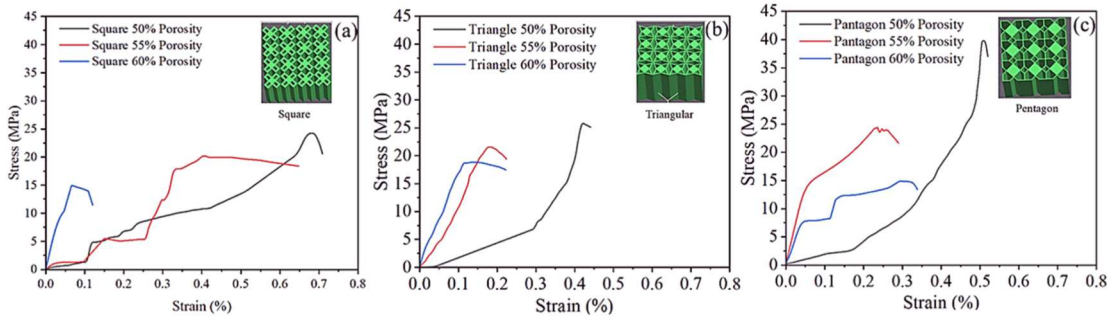

Figure 6. Stress–strain curves of polygon-based lattice unit cells with different porosity (50%, 55% and 60%): (a) Square polygon-based lattice, (b) Triangle polygon-based lattice, and (c) Pentagon polygon-based lattice.

based lattices, correlating lattice design parameters with testing outputs such as load-bearing capacity, energy absorption, and stiffness. It also contributes to optimizing lattice designs for different applications which required lightweight, high-strength, and energy-absorbing materials.

3.2. Polygon-based lattice compressive behavior

Compression testing of each sample yielded a dedicated data file capturing key performance metrics, including the elapsed time, deformation (displacement), applied compressive force, and the strength-to-weight ratio. Unit cell geometry and porosity play vital role in influencing material behavior of support structure such as stress distribution paths, failure initiation points and load-bearing area during load condition. Figure 6 illustrate the compressive behavior of different polygon-based lattice under quasi-static compressive loading. The experimental result shows that the pentagon polygon-based lattices provided enhanced mechanical interlocking and more distributed stress pathways due to their extended sidewalls, delaying buckling and failure. The 50% porosity pentagon lattice exhibited a peak compressive strength of 40.1 MPa, which is 62% and 170% higher than the 50% square (24.2 MPa) and 60% triangle (14.9 MPa) lattices, respectively. The steep drop in stress after peak in the 60% triangle structure indicates brittle-like collapse, while the plateau behavior in the 50% square lattice is indicative of progressive plastic deformation. An increase in porosity from 50% to 60% reduced the porosity by approximately 20%, leading to lower compressive modulus and earlier onset of local buckling. Despite lower strength, the 50% square lattice achieved a total strain of ~0.7, suggesting superior energy absorption under quasi-static loading. These findings align with the Gibson-Ashby model, where compressive strength scales with the square of porosity ($\sigma \propto \rho^2$), explaining the strength reduction at higher porosity.

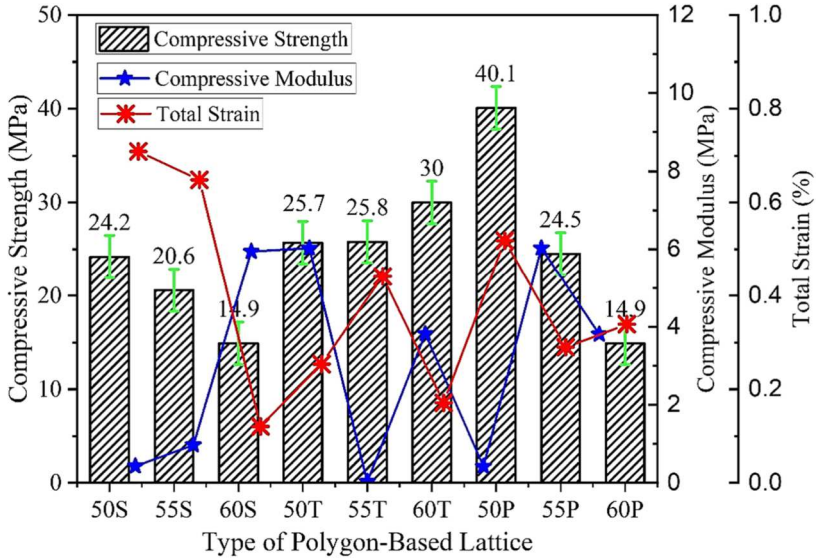

Figure 7. Comparison of compressive strength, compressive modulus, and total strain for different polygon-based lattice structures with varying porosities (50%, 55%, and 60%) and geometries (S: Square, T: Triangle, P: Pentagon).

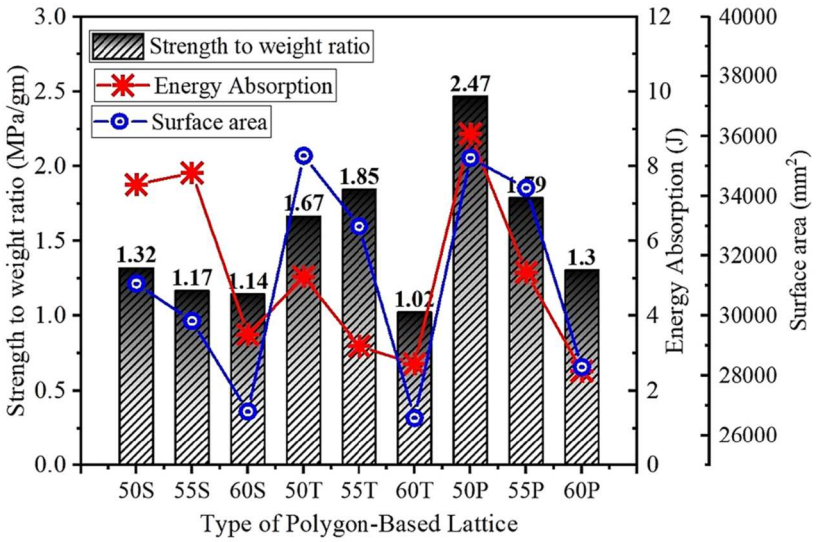

Figure 8. Strength-to-weight versus density and energy absorption.

Figure 7 presents a comparative analysis of compressive strength, compressive modulus, and total strain for polygon-based lattice structures with varying porosities (50%, 55%, and 60%) and geometries—square (S), triangle (T), and pentagon (P). The bar chart shows that the pentagon-based lattice with 50% porosity (50P) achieves the highest compressive strength of 40.1 MPa, indicating its superior load-bearing capability. In contrast, the square and pentagon lattices at 60% porosity (60S and 60P) show the lowest compressive strength of 14.9 MPa, highlighting the weakening effect of increased porosity. Compressive modulus values (blue line) follow a similar trend, with significant reductions at higher porosity levels, particularly noticeable in the 60T and 60S samples. Total strain (red line) appears inversely related to modulus and strength in several cases, with 50S and 55S exhibiting high strain values (>0.8%), suggesting more ductile deformation behavior. Conversely, 60S and 60P have both low strength and strain, implying early brittle failure or structural collapse. This figure illustrates that geometry and porosity significantly influence the mechanical response of lattice structures, with the pentagon-based lattice at lower porosity providing the most favorable balance of strength and stiffness.

Figure 8 presents the relationship between lattice density and strength-to-weight ratio for three distinct lattice configurations square, triangular, and pentagonal each examined at three porosity levels. The square lattice exhibited the lowest mechanical performance among the tested geometries. Specifically, the strength-to-weight ratio for the square lattice at 60% porosity was 1.14 MPa g^{-1}, increasing marginally to 1.17 MPa g^{-1} at 55%, and reaching a maximum of 1.32 MPa g^{-1} at 50% porosity. In contrast, the pentagonal lattice

demonstrated a more pronounced improvement with decreasing porosity. The strength-to-weight ratio increased from 1.30 MPa g^{-1} at 60% porosity to 1.79 MPa g^{-1} at 55%, and peaked at 2.47 MPa g^{-1} for 50% porosity representing the highest value observed across all configurations.

These results indicate a strong correlation between porosity and structural efficiency under compressive loading. As the density increases (i.e., lower porosity), the material provides greater resistance to deformation and failure, resulting in higher strength-to-weight ratios. This trend underscores the critical role of geometric design and porosity control in optimizing lattice performance for lightweight structural applications. The triangular lattice showed a more favorable mechanical response. The strength-to-weight ratio at 60% porosity averaged 1.02 MPa g^{-1}, increasing substantially to 1.67 MPa g^{-1} at 50%, and reaching a maximum of 1.85 MPa g^{-1} at 55% porosity. The analysis of energy absorption and surface area across different lattice configurations reveals notable trends. Pentagonal lattices exhibit the highest energy absorption at 50% porosity, which corresponds with their superior strength-to-weight ratio, indicating enhanced mechanical efficiency at lower porosity levels. In contrast, triangular lattices demonstrate a pronounced peak in energy absorption at 55% porosity, suggesting an optimal balance between density and mechanical performance in this configuration. Square lattices consistently show lower energy absorption values across all porosity levels, reflecting their relatively weaker performance under compressive loading. Additionally, surface area tends to decrease with increasing porosity across all lattice types, with the highest values observed for triangle-based lattices at 50% porosity, likely contributing to their improved energy dissipation capacity.

3.3. Simulation deformation behavior

Figure 9 illustrates the mechanical response of square-patterned lattice structures at increasing porosity levels (50%, 55%, and 60%) under compressive load, as analyzed through finite element simulations. For the square lattice structures, the simulation results revealed a clear influence of porosity on deformation and stress distribution. At 50% porosity, the structure exhibited a maximum total deformation of 0.739 mm and a maximum principal stress of 46.36 MPa, with stress distributed relatively uniformly, indicating efficient load transfer. When the porosity increased to 55%, the maximum deformation rose to 0.863 mm, while the maximum principal stress reduced to 35.54 MPa; however, stress concentration zones began to appear, reflecting a decline in structural integrity. At 60% porosity, the deformation further increased to 1.269 mm, accompanied by a sharp rise in maximum stress to 160.0 MPa, highlighting severe stress localization that may trigger premature failure. At 60% porosity, the structure shows the maximum stress (160.0 MPa) which highlights severe stress localization and potential sites for premature failure. Overall, increasing porosity in the square lattice reduces both stiffness and strength, with the 50% porosity model offering the most favorable mechanical behavior under compressive loads. These results align with experimental data, highlighting the importance of porosity control in the design of lattice-based structures for load-bearing applications.

In figure 10, the triangular-based lattice structures demonstrate a clear dependence of mechanical performance on porosity. At 50% porosity, the lattice exhibits minimal total deformation (0.8803 mm) and a relatively low maximum principal stress of 36.587 MPa. Increasing the porosity to 55% results in a slightly lower deformation (0.8325 mm) but a notable increase in stress capacity to 41.19 MPa, suggesting an optimal porosity for stress distribution and energy absorption. However, at 60% porosity, the structure deforms more significantly (1.3086 mm), despite reaching the highest stress level among the three (46.748 MPa). This indicates that although the structure can withstand greater stress at 60% porosity, it undergoes higher deformation, potentially compromising dimensional stability. Overall, the 55% porosity configuration offers a balance between load-bearing capacity and deformation resistance, making it a promising choice for applications requiring both structural stiffness and lightweight design.

Figure 11 presents the mechanical response of the pentagon-based lattices under compressive loading demonstrates a clear correlation between porosity and structural performance. At 50% porosity, the lattice exhibits the least total deformation (0.7235 mm) and the highest maximum principal stress (172.354 MPa), indicating superior load-bearing capability and stiffness. As the porosity increases to 55%, total deformation rises to 0.8523 mm, while the maximum principal stress decreases significantly to 99.816 MPa, reflecting a reduction in structural integrity. At the highest porosity level of 60%, the deformation further increases to 1.2523 mm, and the maximum principal stress drops to 62.351 MPa. This progressive decline in mechanical performance with increasing porosity suggests that lower porosity enhances structural rigidity and stress resistance in pentagonal lattices. These results are consistent with experimental trends and confirm that 50% porosity offers optimal mechanical behavior for the pentagonal configuration.

3.4. Morphological characterization

To investigate the structure and property relationship of the resin lattices, the fracture surfaces were examined using scanning electron microscopy (SEM), as shown in figure 12. One representative sample from each of the

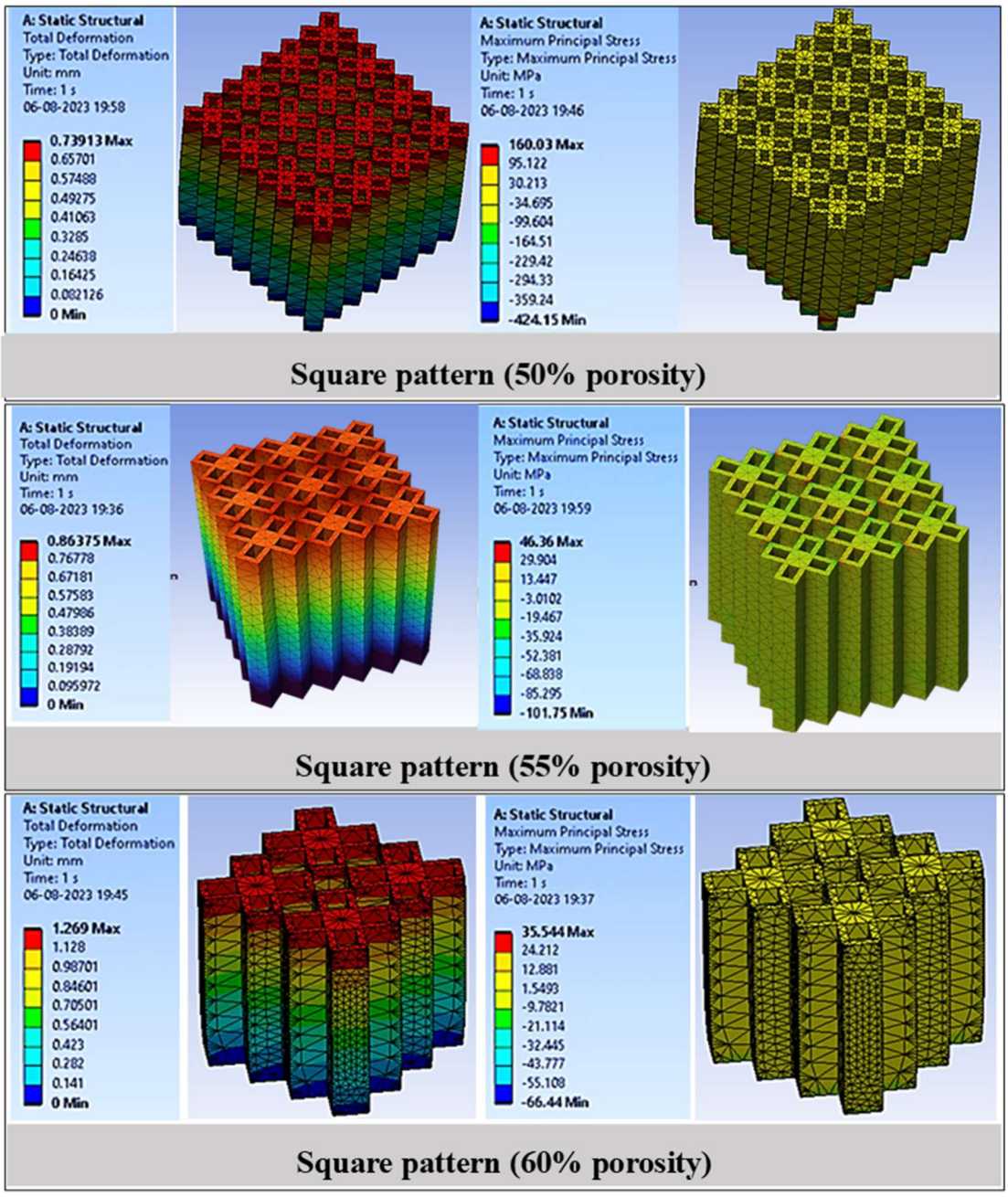

Figure 9. FEA results illustrating total deformation (left) and maximum principal stress (right) for square lattice structures at varying porosity levels.

three lattice types was selected for microstructural analysis. The SLA-printed ABS-like resin lattice exhibits a predominantly brittle fracture with relatively smooth surfaces and occasional voids or agglomerations. These features reflect the typical fracture characteristics of photopolymer resins and highlight the importance of resin homogeneity and printing parameter control for structural consistency. The limited evidence of layer lines or interfacial delamination, indicating good layer-to-layer bonding, which is a positive aspect of the SLA process. The consistency of surface texture across the examined region suggests that the resin curing was largely uniform, although the presence of agglomerates might point to resin particle settlement or mixing issues before printing.

4. Conclusion and future work

This study contributes to the advancement of additive manufacturing by revealing the critical role of unit cell geometry in determining the compressive behavior of lattice structures. Among the configurations tested at different porosity levels, the pentagonal lattice consistently delivered the highest mechanical performance.

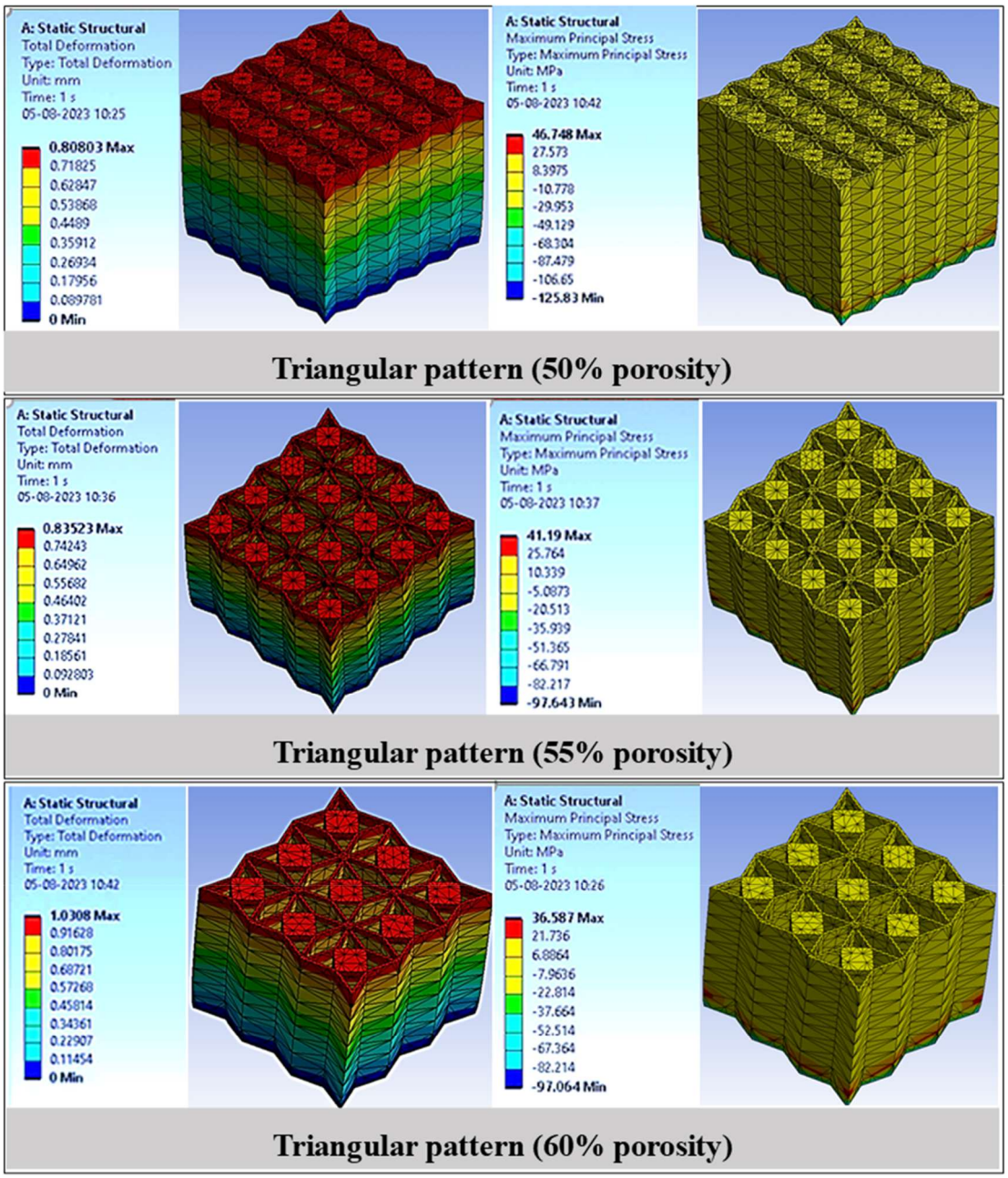

Figure 10. FEA results illustrating total deformation (left) and maximum principal stress (right) for triangular lattice structures at varying porosity levels.

These findings point to its strong potential for structural applications requiring enhanced strength and stability.

- The 50% porosity pentagon lattice exhibited the best compressive performance, with a peak strength of 40.1 MPa, which is 62% higher than the 50% square lattice (24.2 MPa) and 170% higher than the 60% triangle lattice (14.9 MPa). While the triangle lattice showed brittle failure, the square lattice demonstrated better energy absorption, reaching a total strain of ~0.7 under quasi-static loading.
- Based on the comparative results from deformation and stress analyses, the pentagon lattice at 50% porosity demonstrated superior performance with a 71.5% lower total deformation and 371% higher maximum stress compared to the triangular lattice at the same porosity. At 60% porosity, the triangular lattice exhibited a 4.8% higher deformation and a 25.2% lower stress than the pentagonal pattern.
- As per simulation data, the pentagonal lattice at 50% porosity shows the highest performance with ~370% higher maximum stress and ~89% lower deformation compared to the triangular lattice at the same porosity. As porosity increases to 60%, the pentagonal design experiences a 64% drop in stress and 73% rise

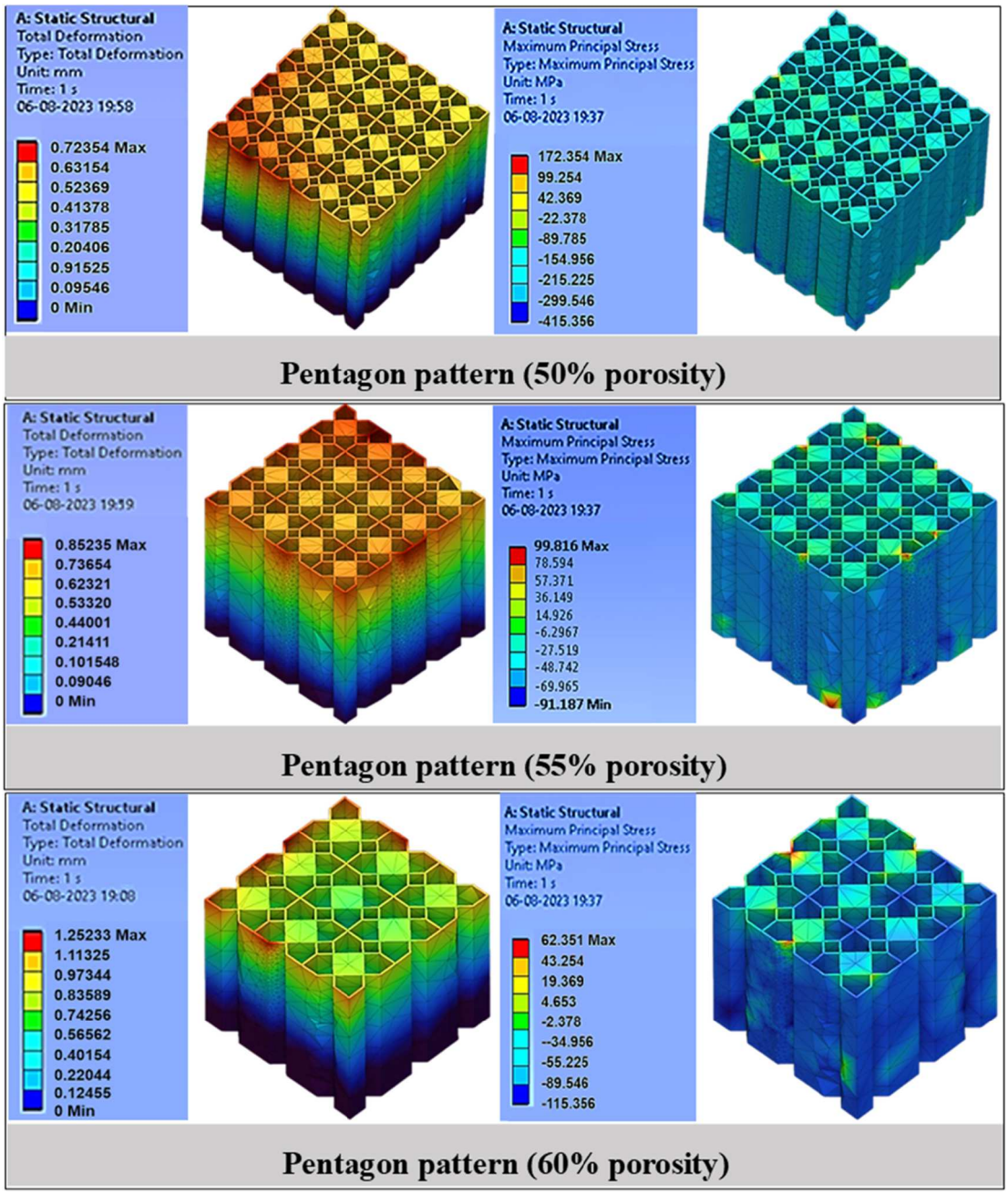

Figure 11. FEA results illustrating total deformation (left) and maximum principal stress (right) for pentagon lattice structures at varying porosity levels.

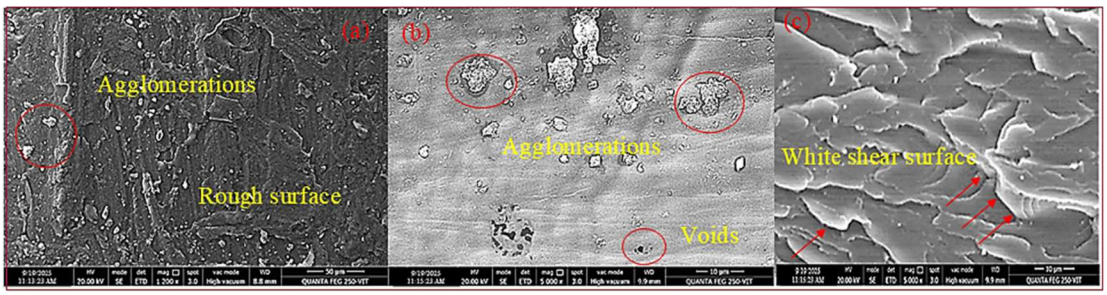

Figure 12. Fracture surface morphology of different fracture struts in different collapse regions under scanning electron microscopy (SEM).

in deformation. In contrast, triangular lattices exhibit more stable stress distribution but ~35%–50% lower strength overall. Thus, the pentagonal lattice, especially at 50% porosity, offers significantly superior load-bearing capability.

- The printed lattice exhibits brittle fracture with smooth surfaces and strong interlayer bonding. Uniform curing is observed, though minor agglomerates indicate possible resin mixing issues

As part of future research, the central solid square will be substituted with other polygonal shapes such as pentagons and hexagons to explore their effects on mechanical properties and enhance the understanding of geometry-dependent performance in lattice structures.

Acknowledgments

Data availability statement

All data that support the findings of this study are included within the article.

Availability of data and materials

On request, the corresponding authors will provide all information and materials necessary to produce the findings in this study.

Declarations of competing interests

Ethical approval

Not applicable.

Competing interests

The authors declare no competing interests.

Author contributions

Ganesh Chouhan 0000-0002-1098-5793
Conceptualization (lead), Methodology (lead), Project administration (lead), Writing – original draft (lead)

Rupesh Chalisgaonkar
Formal analysis (equal), Resources (equal)

Anshuman Purohit
Data curation (equal), Resources (equal)

Avinash Kumar Namdeo 0000-0001-9486-0412
Formal analysis (equal), Investigation (supporting), Software (equal)

Deepak Kumar Yaduwanshi
Formal analysis (lead), Methodology (equal), Visualization (equal)

Kunal Gandvane 0009-0008-0023-7063
Methodology (equal), Software (lead), Visualization (equal)

Prveen Bidare 0000-0003-2852-3498
Project administration (equal), Writing – review & editing (equal)

References

[1] Ashby M F 2016 *Materials Selection in Mechanical Design* 5th edn (Butterworth-Heinemann)
[2] Peng X *et al* 2022 Bioinspired strategies for excellent mechanical properties of composites *J. Bionic Eng.* **19** 1203–28
[3] Huang S H, Liu P, Mokasdar A and Hou L 2013 Additive manufacturing and its societal impact: a literature review *Int. J. Adv. Manuf. Technol.* **67** 1191–203
[4] SakshiKokil-Shah, Sur A, Darvekar S and Shah M 2021 Recent advancements of micro-lattice structures: application, manufacturing methods, mechanical properties, topologies and challenges *Arab. J. Sci. Eng.* **46** 11587–600
[5] Ha N S and Lu G 2020 A review of recent research on bio-inspired structures and materials for energy absorption applications *Composition B* **181** 107496
[6] Doodi R and Balamurali G 2023 Experimental and analytical investigation of bio-inspired lattice structures under compressive loading *Eng. Res. Express* **5** 35035
[7] Ramakrishna D and Murali G B 2023 Bio-inspired 3D-printed lattice structures for energy absorption applications: a review *Proc. Inst. Mech. Eng. J* **237** 503–42
[8] Wang P *et al* 2021 Bioscaffolds embedded with regulatory modules for cell growth and tissue formation: a review *Bioact. Mater.* **6** 1283–307
[9] Sharma D and Hiremath S S 2022 Bio-inspired repeatable lattice structures for energy absorption: experimental and finite element study *Compos. Struct.* **283** 115102
[10] Siddique S H *et al* 2022 Lessons from nature: 3D printed bio-inspired porous structures for impact energy absorption—a review *Addit. Manuf.* **58** 103051
[11] Jaradat M, Soliman E and Taha M R 2023 3D-printed bio-inspired mechanically interlocked viscoelastic dampers for energy dissipation *Mater. & Des.* **228** 111826
[12] Zluhan B *et al* 2025 Design, defect analysis, compressive strength and surface texture characterization of Laser Powder Bed Fusion processed Ti6Al4V lattice structures *J. Mater. Res. Technol.* **35** 2914–33
[13] Chen W *et al* 2015 Static and dynamic mechanical properties of expanded polystyrene *Mater. Des.* **69** 1–21
[14] Zou M *et al* 2016 A bionic method for the crashworthiness design of thin-walled structures inspired by bamboo *Thin-Walled Struct.* **101** 222–30
[15] Ma J, Chen W, Zhao L and Zhao D 2008 Elastic buckling of bionic cylindrical shells based on bamboo *J. Bionic Eng.* **5** 231–8
[16] Hu D *et al* 2019 Energy-absorption characteristics of a bionic honeycomb tubular nested structure inspired by bamboo under axial crushing *Composition B* **162** 21–32
[17] Xiang J and Du J 2017 Energy absorption characteristics of bio-inspired honeycomb structure under axial impact loading *Mater. Sci. Eng. A* **696** 283–9
[18] Yin H *et al* 2015 Crushing analysis and multi-objective optimization design for bionic thin-walled structure *Mater. & Des.* **87** 825–34
[19] Yin H *et al* 2016 Multi-objective robust optimization of foam-filled bionic thin-walled structures *Thin-Walled Struct.* **109** 332–43
[20] Ha N S, Lu G and Xiang X 2019 Energy absorption of a bio-inspired honeycomb sandwich panel *J. Mater. Sci.* **54** 6286–300
[21] Xia H, Sun Q and Liu Y 2022 Energy absorption characteristics of bio-inspired honeycomb column thin-walled structure under low strain rate uniaxial compression loading *Energies* **15** 6957
[22] Zhang L, Bai Z and Bai F 2018 Crashworthiness design for bio-inspired multi-cell tubes with quadrilateral, hexagonal and octagonal sections *Thin-Walled Struct.* **122** 42–51
[23] An X and Fan H 2016 Hybrid design and energy absorption of luffa-sponge-like hierarchical cellular structures *Mater. & Des.* **106** 247–57
[24] Bührig-Polaczek A *et al* 2016 Biomimetic cellular metals—using hierarchical structuring for energy absorption *Bioinspiration & Biomimetics* **11** 45002
[25] Tane M, Zhao F, Song Y H and Nakajima H 2014 Formation mechanism of a plateau stress region during dynamic compression of porous iron: interaction between oriented cylindrical pores and deformation twins *Mater. Sci. Eng. A* **591** 150–8
[26] Rhee H *et al* 2015 Structure-property responses of bio-inspired synthetic foams at low and high strain rates *Sci. Eng. Compos. Mater.* **22** 365–73
[27] Yi Z *et al* 2019 Density gradient tailoring of aluminum foam-filled tube *Compos. Struct.* **220** 451–9
[28] Yang X *et al* 2017 Crashworthiness investigation of the bio-inspired bi-directionally corrugated core sandwich panel under quasi-static crushing load *Mater. & Des.* **135** 275–90
[29] Doodi R, Harsha K S, Gunji B M and Mahapatra G S 2024 Energy absorption capacity of bio-inspired honeycomb integrated beetle elytron plates *Eng. Proc.* **66**
[30] Sun Z *et al* 2016 On compressive properties of composite sandwich structures with grid reinforced honeycomb core *Composition B* **94** 245–52
[31] Peng C *et al* 2021 3D printed sandwich beams with bioinspired cores: mechanical performance and modelling *Thin-Walled Struct.* **161** 107471
[32] Pelanconi M and Ortona A 2019 Nature-inspired, ultra-lightweight structures with gyroid cores produced by additive manufacturing and reinforced by unidirectional carbon fiber ribs *Materials (Basel)* **12** 4134
[33] Rice C and Tan K T 2019 Horse hoof inspired biomimetic structure for improved damage tolerance and crack diversion *Compos. Struct.* **220** 362–70
[34] Ghazlan A *et al* 2020 Performance of a 3D printed cellular structure inspired by bone *Thin-Walled Struct.* **151** 106713
[35] Zorzetto L and Ruffoni D 2019 Wood-inspired 3D-printed helical composites with tunable and enhanced mechanical performance *Adv. Funct. Mater.* **29** 1805888
[36] Wang B *et al* 2019 Lessons from the ocean: whale baleen fracture resistance *Adv. Mater.* **31**
[37] Zhang X *et al* 2019 Compression properties of metal beetle elytron plates and the elementary unit of the trabecular-honeycomb core structure *J. Sandw. Struct. & Mater.* **21** 2031–41
[38] Vlasea M, Pilliar R and Toyserkani E 2015 Control of structural and mechanical properties in bioceramic bone substitutes via additive manufacturing layer stacking orientation *Addit. Manuf.* **6** 30–8

[39] Peng M et al 2019 3D printing of ultralight biomimetic hierarchical graphene materials with exceptional stiffness and resilience *Adv. Mater.* **31** 1902930
[40] Gibson L J, Ashby M F, Schajer G S and Robertson C I 1997 The mechanics of two-dimensional cellular materials *Proc. R Soc. London A Math Phys. Sci.* **382** 25–42
[41] Chouhan G and Bala Murali G 2023 Uniform and graded bio-inspired gyroid lattice: effects of post-curing and print orientation on mechanical property *Proc. Inst. Mech. Eng. L* **238** 810–28